Available online at www.sciencedirect.com
SCIENCE DIRECT
International Journal of Heat and Fluid Flow 27 (2006) 721–729
International Journal of HEAT AND FLUID FLOW
www.elsevier.com/locate/ijhff

The influence of disturbances carried by periodically incoming wakes on the separating flow around a turbine blade

Jan G. Wissink [a,*], Wolfgang Rodi [a], Howard P. Hodson [b]

[a] Institute for Hydromechanics, University of Karlsruhe, Kaiserstrasse 12, D-76128 Karlsruhe, Germany
[b] Whittle Laboratory, University of Cambridge, Madingley Road, Cambridge CB3 0D, UK

Available online 23 March 2006

Abstract

The effect of fluctuations caused by periodically incoming wakes on the separating flow around a turbine blade are studied using direct numerical simulations of incompressible flow—at a Reynolds number of $Re = 51{,}831$—in the T106A low-pressure turbine cascade. To be able to differentiate between the effect of small-scale fluctuations and large-scale fluctuations, in one of the simulations small-scale disturbances have been removed from the wake before it enters the computational domain. It is shown that the large-scale disturbance, associated with the presence of the mean wake, triggers the Kelvin–Helmholtz instability of the separated shear layer along the downstream half of the suction side, which is also observed in experiment. On the suction side, the small-scale fluctuations carried by the wakes are found to seed the transition to turbulence of the rolled-up shear layer flow, while on the pressure side the fluctuations are responsible for the formation of longitudinal vortical structures [Wu, X., Durbin, P.A., 2001. Evidence of longitudinal vortices evolved from distorted wakes in a turbine passage. J. Fluid Mech. 446, 199–228]. Finally, the production of kinetic energy inside the passage between blades is also found to depend on the presence of fluctuations inside the wakes.

Keywords: Transition; Turbines; Boundary layer separation; Wakes

1. Introduction

In modern jet engines the low-pressure (LP) turbine supplies power to the fan and, sometimes, the first compressor stages. Recent increases in fan diameters require a higher work-output from the LP turbine at reduced rotational speed. Typically, an LP turbine is relatively heavy since it consists of several stages, while its efficiency strongly influences fuel consumption. Hence, even small improvements have a significant effect.

The periodic unsteadiness induced by rotor–stator interaction and the low Reynolds number are characteristic for flow in an LP turbine. Both phenomena directly affect blade boundary layer transition, the tendency to separation, heat transfer and flow losses. Separation of the boundary layer along a turbine blade changes the aerodynamical properties of a blade and might eventually cause mechanical failure. Free-stream fluctuations and incoming wakes, generated by the upstream row of blades, can be employed to passively control this boundary layer separation.

The models used for transition and turbulence in industrial CFD codes are still not sufficiently reliable and universal to accurately predict the complex flow in a turbine cascade. To improve these models both experimental data (Schulte and Hodson, 1998; Stadtmüller, 2002; Stieger and Hodson, 2003; Liu and Rodi, 1994a,b) and data from direct numerical simulations (DNS) (Kalitzin et al., 2002; Wissink, 2003; Wu and Durbin, 2001) and large-eddy simulations (LES) (Michelassi et al., 2002, 2003; Raverdy et al., 2003) can be employed. Compared to experiments, the main advantage of DNS is the possibility to extract quantities at any location without disturbing the flow. This detailed picture of the flow might be of great help to identify, for instance, physical mechanisms that play a role in

* Corresponding author. Tel.: +49 721 608 3536; fax: +49 721 608 2202.
E-mail address: wissink@ifh.uni-karlsruhe.de (J.G. Wissink).

0142-727X/$ - see front matter © 2006 Elsevier Inc. All rights reserved.
doi:10.1016/j.ijheatfluidflow.2006.02.016

Nomenclature

b	half-width of mean wake
C	chord-length
C_p	mean wall static-pressure coefficient $C_p = \frac{\overline{p}-\overline{p}_{\text{ref}}}{1/2\overline{u}_{\text{ref}}^2}$
CFD	computational fluid dynamics
d	diameter of the cylinders
DNS	direct numerical simulation
k	fluctuating kinetic energy made dimensionless using U^2
K	acceleration parameter $K = \frac{\nu}{U_e^2}\frac{\partial U_e}{\partial s}$
KH	Kelvin–Helmholz
L	axial chord-length
LES	large-eddy simulation
LP	low pressure
p	modified static pressure made dimensionless using U and L
p_{ref}	modified static pressure in point of reference
P	pitch between blades
Re	Reynolds number based on U and L
Re_1	Reynolds number based on U and C
Re_{exit}	Reynolds number based on C and exit conditions
t	time made dimensionless using L/U
T	wake-passing period
U	mean inflow velocity
U_{bar}	vertical velocity of the cylinders
U_{def}	mean velocity deficit of the wake
U_e	free-stream velocity
u	velocity-component in the axial direction
u_{ref}	velocity magnitude in point of reference
u_τ	friction velocity made dimensionless using U
v	velocity-component in the normal direction
w	velocity-component in the spanwise direction
$\overline{f}$	mean of f
f'	fluctuating part of f
$\langle f \rangle$	phase-averaged part of f ($\langle f \rangle = f - f'$)
Greek symbols	
α	inflow angle
λ_2	second largest eigenvalue of the sum of the squares of the symmetric and antisymmetric parts of the velocity gradient tensor
ϕ	phase
ν	kinematic viscosity
ω_z	spanwise component of the vorticity

the transition to turbulence. Unfortunately, because of computational restrictions, the usage of DNS is still limited to relatively simple geometries.

Compared to a wall-resolved DNS, a wall-resolved LES only allows a reduction of the number of grid points by approximately a factor of ten. A direct comparison of LES and DNS by Michelassi et al. (2002) showed that LES provides a fair description of the flow, though boundary layer transition was found to be affected by a lack of resolution of both the boundary layer and the free-stream fluctuations. As a consequence, the usefulness of LES as a tool to obtain quality data with which to improve industrial CFD models for transition is rather limited.

In the experimental work performed by Stieger and Hodson (2003), the interaction of a wake with the separated suction side boundary layer of the T106 turbine blade was studied. The experiments suggested that the impinging wake was responsible for triggering a Kelvin–Helmholtz (KH) instability. As a consequence, the separated boundary layer rolled up into several rolls of re-circulating flow. Unfortunately, in the experiments it was extremely difficult to differentiate between the mean effect of the wake as a negative jet and the effect of the small-scale fluctuations carried by the wakes. To further investigate these effects on the transition to turbulence of the separated suction side boundary layer direct numerical simulations (DNS) of separating flow in the linear T106 low-pressure (LP) turbine cascade with periodically incoming wakes have been performed, using a set-up similar to the one used in the experiments.

To be able to study the effect of fluctuations carried by the incoming wakes on boundary layer separation along the suction side of the turbine blade, it was decided to perform a similar thought experiment as reported earlier for a flat plate boundary layer flow without separation by Wu et al. (1999). In one of two simulations reported in this paper, all fluctuations were removed from the wake before it entered the computational domain. At the inlet, located at $x/L = -0.5$, the velocity-deficit $U_{\text{def}} = 0.25U$ and half-width $b = 0.03L$ of the fluctuation-free wakes exactly match the mean velocity deficit and half-width of the realistic wakes used in the reference DNS (Wissink, 2003). The Reynolds number of the present flow problem, based on the mean inflow velocity U and the axial chord-length L (see Fig. 1), was chosen to be $Re = 51{,}831$. This corresponds to an exit Reynolds number, based on the mean outlet velocity and chord-length, C, of $Re_{\text{exit}} \approx 92{,}000$. The Reynolds number of $Re_1 = 60{,}000$, referred to in Wissink (2003), is based upon the chord-length and the mean inflow velocity. The pitch between blades is $P = 0.9306L$, and the distance between the wake-generating cylinders is $\frac{1}{2}P$. The cylinders of diameter $d = 0.02327L$ move in the negative y-direction with velocity $U_{\text{bar}} = 0.4089U$. This results in a period of $T = 1.138L/U$, corresponding to the time needed for the cylinders to perform a vertical sweep over a distance $\frac{1}{2}P$. In the spanwise direction and in the vertical direction, upstream and downstream of the blades, periodic boundary conditions were prescribed. The spanwise size of the computational domain was $0.20L$. Along the surface of the blades no-slip boundary conditions were

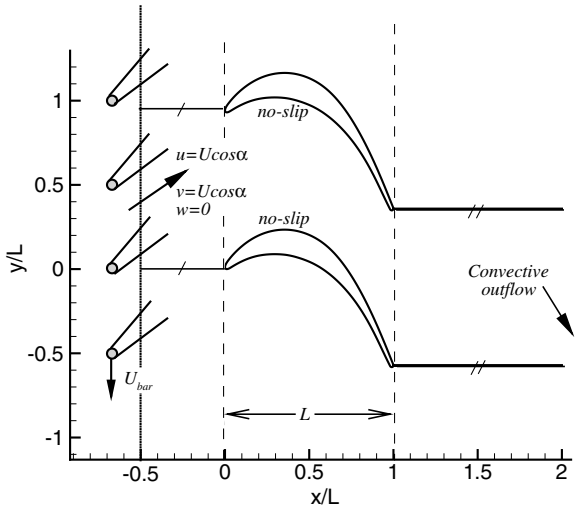

Fig. 1. Cross-section at midspan of the computational domain.

employed, while at the outlet a convective outflow boundary condition was used. The realistic wakes and fluctuation-free wakes, respectively, were introduced at the inlet, superposed on a uniform flow-field $(u, v, w) = U(\cos\alpha, \sin\alpha, 0)$, where $\alpha = 45.5°$. The wake-data have been kindly made available by Xiauhua Wu and Paul Durbin of Stanford University. Their statistical properties are described in Wu et al. (1999). An overview of the performed simulations is provided in Table 1. The quality of the computational mesh used in the simulations was assessed earlier in Wissink (2003). This paper reports on a grid-refinement study of Simulation A, in which also the spanwise size of the computational domain is varied.

The computations were performed on the Hitachi SR8000-F1 at the Leibniz Computing Centre (LRZ) in Munich, using 64 processors. The 3D, incompressible Navier–Stokes equations were discretised using a finite-volume approach, employing a central, second-order accurate discretisation in space combined with a three-stage Runge–Kutta method for the time-integration. To avoid a decoupling of the pressure field and the velocity field owing to the collocated variable arrangement used in the code, the momentum interpolation procedure of Rhie and Chow (1983) is applied. A more detailed description of the code is provided in Breuer and Rodi (1996). After allowing the flow to develop for at least five periods, phase-averaging has been performed for ten periods in Simulation A and 15 periods in Simulation B. To speed up the convergence, phase-averaging is combined with averaging the data in the homogeneous spanwise direction.

Table 1
Overview of the performed simulations, wake half-width is $0.03L$ and mean wake velocity deficit is $0.25U$

Simulation	Grid	Fluctuations in wake
A	$1014 \times 266 \times 64$	Yes
B	$1014 \times 266 \times 64$	No

2. Results

Fig. 2 shows that the time-averaged wall static-pressure coefficient C_p obtained in the two simulations listed in Table 1 is generally in good agreement. Only along the downstream half of the suction side, the kink in the C_p distribution of Simulation A—identified by the arrow—is found to be slightly more pronounced than in Simulation B. This result indicates that the time-averaged separation bubble in Simulation A is marginally larger than the bubble obtained in Simulation B. This is somewhat surprising since increasing the amount of fluctuations usually leads to a reduction in size of the separation bubble.

The boundary layer separation is induced by the adverse streamwise pressure gradient along the downstream half of the suction side. While in Simulation A incoming wakes are found to periodically completely suppress separation (see Wissink, 2003), in Simulation B only a periodic reduction in size of the separated area is obtained (see also Fig. 9).

To further investigate the effects of small-scale free-stream fluctuations carried by the wakes on the static-pressure distribution on the suction side, in Fig. 3, the phase-averaged wall static-pressure distribution $\langle p \rangle - \langle p \rangle|_{x/L=0}$ has been plotted for four phases $\phi = 0, 1/4, 2/4, 3/4$. The graph at $\phi = 3/4$ clearly shows the presence of huge fluctuations in the static pressure in Simulation B, which have approximately twice the amplitude of the corresponding fluctuations from Simulation A. These static-pressure fluctuations somewhat upstream of the trailing edge are a reflection of the presence of rolls of re-circulating flow such as observed for Simulation B in Fig. 9. While in Simulation B the amplitude of the pressure fluctuations slowly declines as they are convected downstream—as can be seen in the series of snapshots at $\phi = 3/4$, $\phi = 0$, $\phi = 1/4$—in Simulation A the pressure fluctuations are found to have vanished between $\phi = 3/4$ and $\phi = 0$. Hence, we can conclude that the small-scale fluctuations carried by the wakes of Simulation A are able to significantly damp the occurrence of static-pressure fluctuations along the

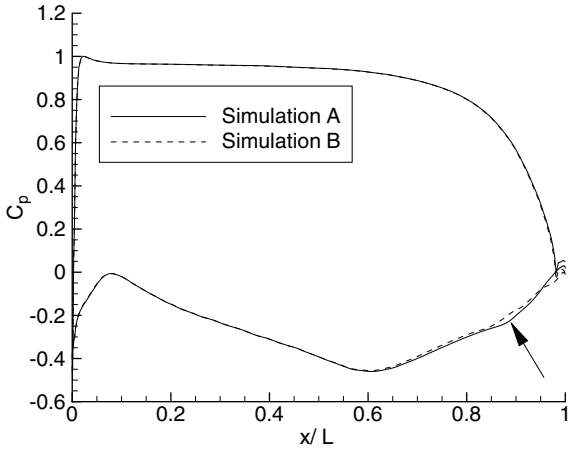

Fig. 2. Mean wall static-pressure coefficient $C_p = \frac{2(\overline{p}-\overline{p}_{\mathrm{ref}})}{\overline{u}^2_{\mathrm{ref}}}$.

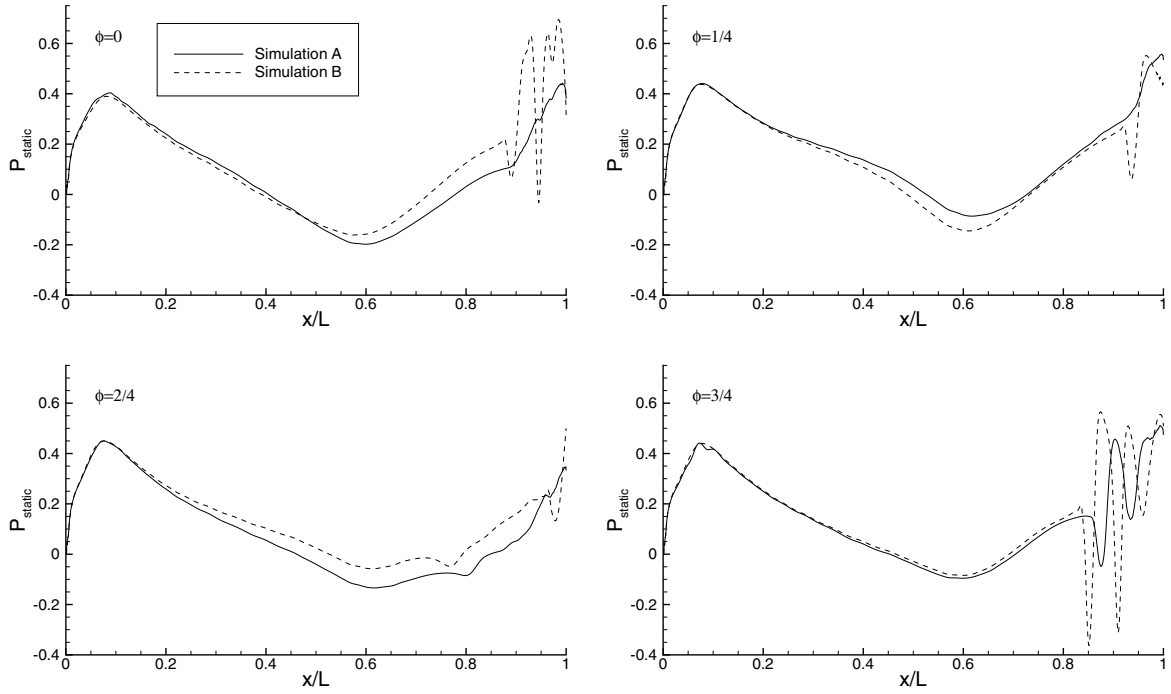

Fig. 3. Phase-averaged wall static-pressure $\langle p\rangle - \langle p\rangle|_{x/L=0}$ on the suction side of the blade at $\phi = 0, 1/4, 2/4, 3/4$.

downstream half of the suction side. As already noted above, there is a close connection between the static-pressure fluctuations and the occurrence of the rolls of re-circulating flow. It will be shown later in the paper that the damping of the static-pressure fluctuations is, in fact, directly related to the destruction of rolls of re-circulating flow by the small-scale fluctuations (see also Fig. 8).

In Fig. 4 contours of the phase-averaged spanwise vorticity are shown in the passage between blades of Simulation B at four different phases. The fact that the contours of the wakes appear to be very smooth is a reflection of the fact that the wakes employed in the simulation are free of small-scale disturbances. In other words: the phase-averaged flow fields tend to be quite similar to the instantaneous flow fields. As the wake approaches the turbine blade, it wraps itself around the leading edge. Immediately downstream of the leading edge, the wake is severely stretched by the accelerating wall-parallel flow as it approaches the suction side of the blade. This stretching of the wake significantly damps any disturbances carried by the wake and simultaneously reduces the impact of the impingement of the wake in this region. Further downstream along the suction side, the angle with which the wake impinges on the suction side continues to be very small. Along the pressure side, the angle tends to become smaller with decreasing distance to the trailing edge. As shown in Wu and Durbin (2001), wakes are passively convected by the free-stream. Because of the absence of disturbances, in Simulation B the folding and stretching of the wake by the free-stream velocity is very clearly illustrated.

The contours of the phase-averaged kinetic energy at $\phi = 2/8$ displayed in Fig. 5 show a result which is characteristic for all phases. Fig. 5a illustrates that in Simulation A kinetic energy is produced at the apex of the wake as it is convected through the passage between wakes. This was also found in the experiments performed by Stieger and Hodson (2005). The absence of a similar peak at the apex of the averaged wake in Simulation B (see Fig. 5b) proves that small-scale disturbances carried by the wakes are needed to seed this production of kinetic energy. Another difference between the two simulations can be observed in the wake generated by the turbine blade. The absence of large-scale structures in the phase-averaged near wake in Simulation A is explained by the fact that the fluctuating kinetic energy produced in the suction side boundary layer, immediately upstream of the trailing edge, hinders the formation of such vortical structures. In contrast to this, large structures are found to be present in the phase-averaged wake of Simulation B, where there is virtually no production of fluctuating kinetic energy in the suction side boundary layer. This is, for instance, evidenced by the snapshot at $\phi = 2/8$ shown Fig. 5b and is also observed at the other phases (see also Fig. 6). Hence, virtually the entire suction side boundary layer in Simulation B remains laminar for all phases. This, however, does not imply that the boundary layer remains undisturbed for all phases. Low-level numerical round-off error may eventually trigger transition also in Simulation B. This is evidenced, for instance, by the high levels of $\langle k\rangle$ in the wake of the turbine blade which are likely to have been seeded by numerical disturbances. Still, the absence or presence of small-scale fluctuations is found to have a significant effect on the boundary layer transition along the downstream half of the suction side.

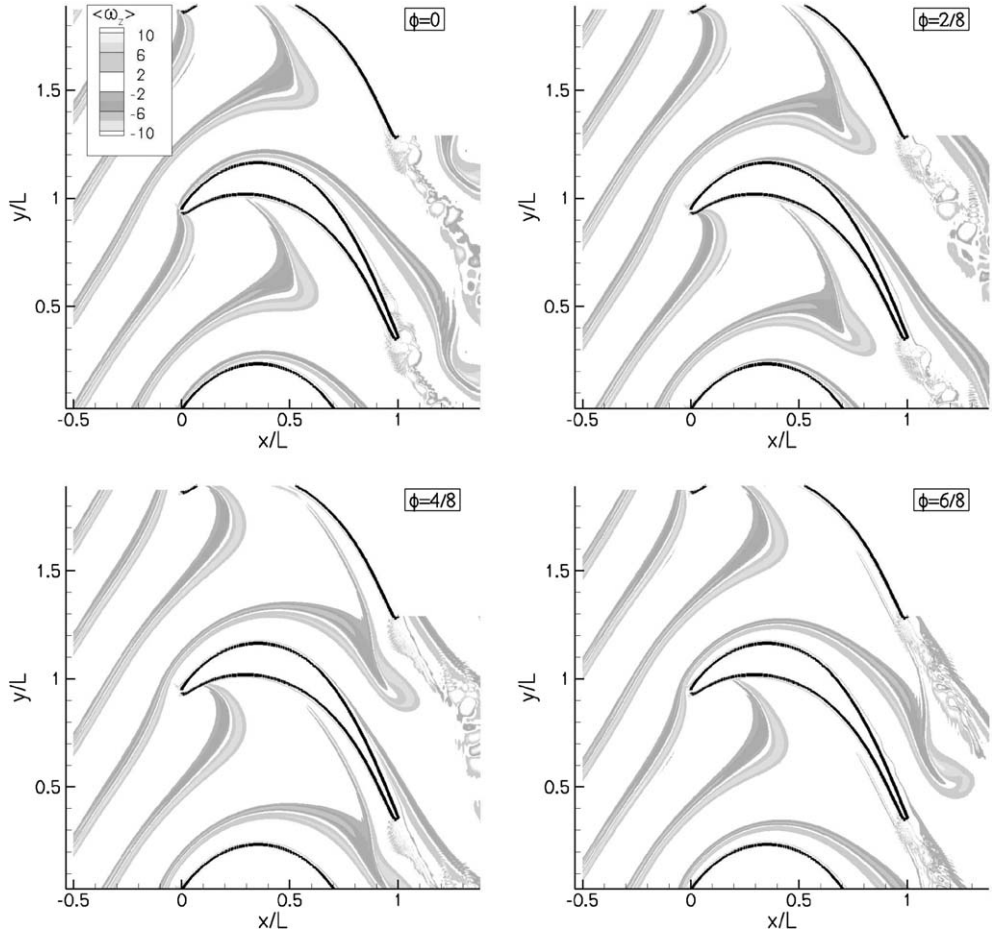

Fig. 4. Contours of the phase-averaged spanwise vorticity $\langle \omega_z \rangle$ at four different phases (Simulation B).

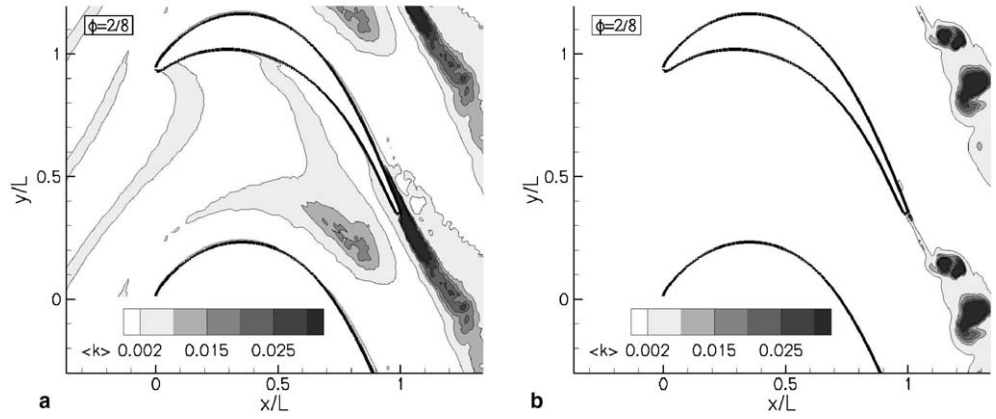

Fig. 5. Contours of the phase-averaged fluctuating kinetic energy $\langle k \rangle$ at $\phi = 2/8$. (a) Simulation A and (b) Simulation B.

In Fig. 6, contours of the phase-averaged spanwise vorticity and the phase-averaged fluctuating kinetic energy at $\phi = 6/8$ are shown for both Simulations A and B for the suction side region near the trailing edge (The actual location of the wake is detailed in Fig. 8). In Simulation A, with small-scale disturbances carried by the wakes, a significant amount of fluctuating kinetic energy is found to be produced inside the rolled-up shear layer. In the absence of these small-scale disturbances (Simulation B), no fluctuating kinetic energy is produced inside the rolled-up shear layer. Instead, the increase in $\langle k \rangle$ is located very close to the trailing edge, which suggests that the location of transition has moved downstream as compared to Simulation A. The rolling-up of the separated shear layer itself is attributed to a Kelvin–Helmholtz (KH) instability which was also clearly found to be present in the experiments of

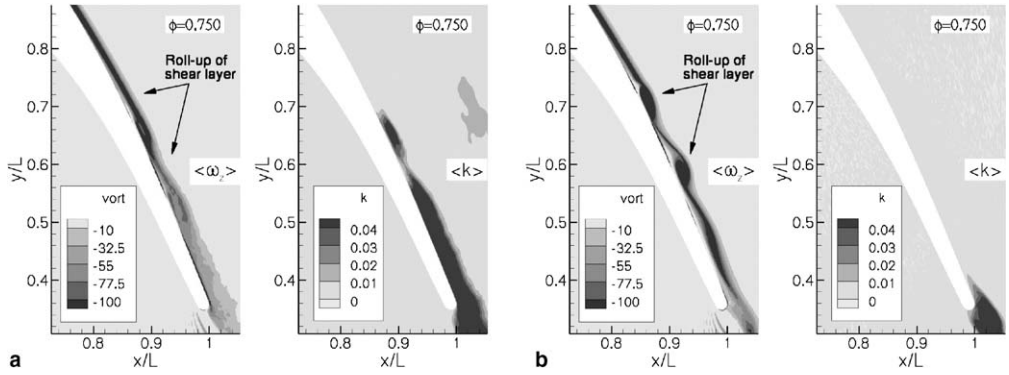

Fig. 6. Contours of the phase-averaged spanwise vorticity $\langle\omega_z\rangle$ (left) and fluctuating kinetic energy $\langle k\rangle$ (right) both at $\phi = 0.750$. (a): Simulation A and (b) Simulation B.

separating flow in the T106A cascade with periodically incoming wakes performed by Stieger et al. (2003) and is illustrated in Fig. 7 (see also Stieger and Hodson, 2003). The figure shows a vector plot and a streak line plot of an instantaneous flow-field near the trailing edge of the suction side. From the experiments mentioned above and from the experiments of the more highly loaded T106C case (reported in Zhang and Hodson, 2004) it was deduced that the pressure/velocity field created by the negative jet—associated with the wake—induces roll-up of the shear layer. When the wake subsequently physically touches the separated boundary layer, small-scale disturbances carried by the wake trigger further transition to turbulence. From the above, we may conclude that there is compelling evidence that the KH instability of the separated shear layer along the downstream half of the suction side is triggered by the low-frequency disturbance associated with the mean part of the impinging wakes, while further transition to turbulence is promoted by small-scale fluctuations carried by the wakes of Simulation A.

For Simulation B, Fig. 8 shows a series of four snapshots of streamlines of the phase-averaged velocity field together with grey-scale contours of the phase-averaged spanwise vorticity which identify the wakes. The figure gives further evidence that the periodically impinging wakes are responsible for triggering the KH instability of the separated shear layer. At $\phi = 4/8$, the wake can be seen to impinge between $x/L = 0.85$ and $x/L = 0.90$. With time, the location of impingement moves farther downstream such that at $\phi = 5/8$, it has reached the region immediately upstream of the trailing edge. Simultaneously, the shear layer is found to roll up into several rolls of re-circulating flow, which are especially clearly visible in the snapshot taken at $\phi = 6/8$. When the wake is no longer impinging, the rolls of re-circulating flow are convected downstream.

A three-dimensional illustration of the dynamics of the suction side boundary layer flow from Simulation B is shown in Fig. 9. Here, snapshots are shown of the spanwise vorticity iso-surface $\omega_z = -150$ near the downstream half of the suction side of Simulation B. The wakes are identified with the grey-scale contours of the instantaneous spanwise vorticity, which are displayed at the back. As in Fig. 8, the wake can be seen to impinge on the suction side boundary layer at $t/T = 10\frac{4}{8}$. Because of this impingement, at $t/T = 10\frac{6}{8}$, the shear layer has rolled up into two separate rolls of re-circulating flow. The figure clearly illustrates that the boundary layer flow remains essentially two-dimensional along most of the downstream half of the suction side. Even inside the rolls of re-circulating flow, no further transition to turbulence can be observed. Only very close to the trailing edge the flow intermittently turns three-dimensional as instabilities are triggered by numerical round-off error (see snapshots at $t/T = 10\frac{2}{8}25, 10\frac{4}{8}$ and $10\frac{6}{8}$). The same instabilities are responsible for the increase in the spanwise averaged fluctuating kinetic energy near the trailing edge as observed in Fig. 6b.

Fig. 10 shows the time-averaged friction velocity u_τ together with the envelope of the phase-averaged u_τ signals along the suction side of the turbine blade for Simulations A and B. Upstream of $x/L = 0.9$, the friction velocity profiles obtained in Simulations A and B are virtually identical. Further downstream a difference can be observed. While in Simulation A the time-averaged friction velocity clearly increases towards the trailing edge, in Simulation B u_τ slightly fluctuates and only assumes values slightly lar-

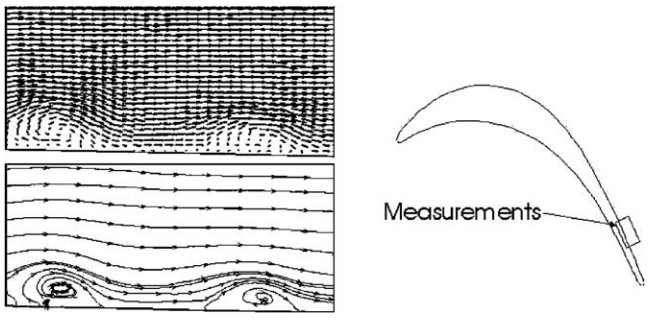

Fig. 7. Experimental evidence of the Kelvin–Helmholtz instability which was found to be intermittently triggered. The upper two graphs show vector and streak lines plots of the instantaneous flow at midspan in the measurement region which is identified by the box below (from Stieger et al., 2003).

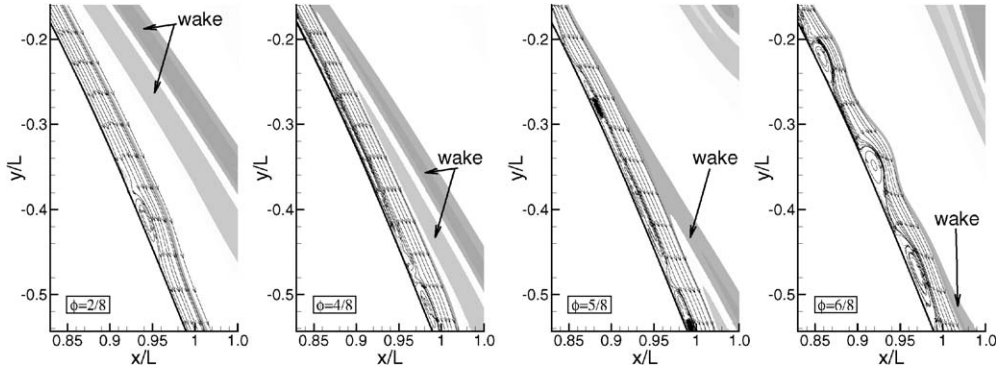

Fig. 8. Simulation B: Phase-averaged snapshots showing streamlines to identify the near-wall velocity field combined with contours of the spanwise vorticity to identify the wakes.

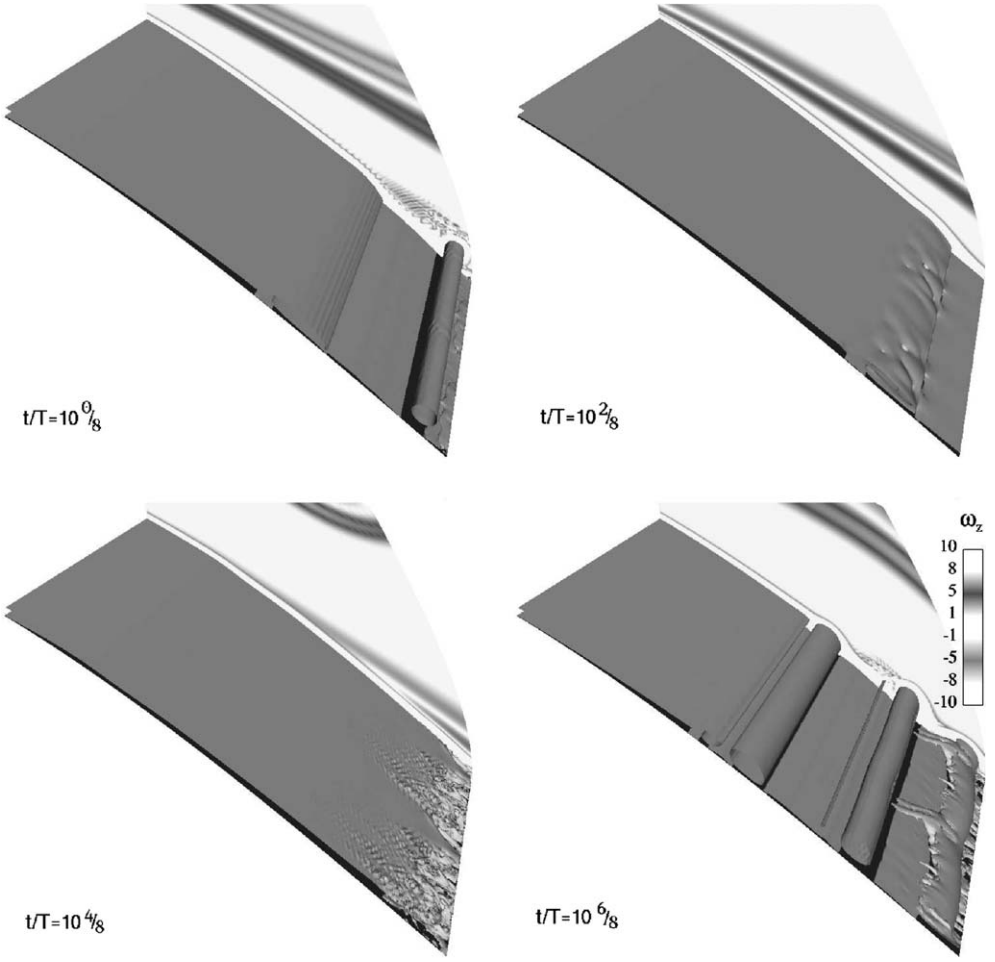

Fig. 9. Simulation B: Snapshots of the spanwise vorticity iso-surface $\omega_z = -150$ at $t/T = 10\frac{0}{8}, 10\frac{2}{8}, 10\frac{4}{8}$ and $10\frac{6}{8}$. The grey-scale contours at the back show the instantaneous spanwise vorticity and identify the wakes. Note that a disturbance-free wake consists of a positive and a negative vortex sheet adjacent to one another.

ger than zero. This difference can be explained from the phase-averaged fluctuating kinetic energy results plotted in Fig. 6a and b. These results witness that the onset of transition of the suction side boundary layer flow in Simulation A is located farther upstream than the onset of transition in Simulation B. The latter boundary layer flow turns transitional only slightly upstream of the trailing edge. The downstream increase in the time-averaged u_τ in Simulation A reflects the fact that the boundary layer flow turns mildly turbulent. While for $x/L < 0.8$ the envelopes of the phase-averaged u_τ signals of Simulations A and B are virtually the same, further downstream significant differences

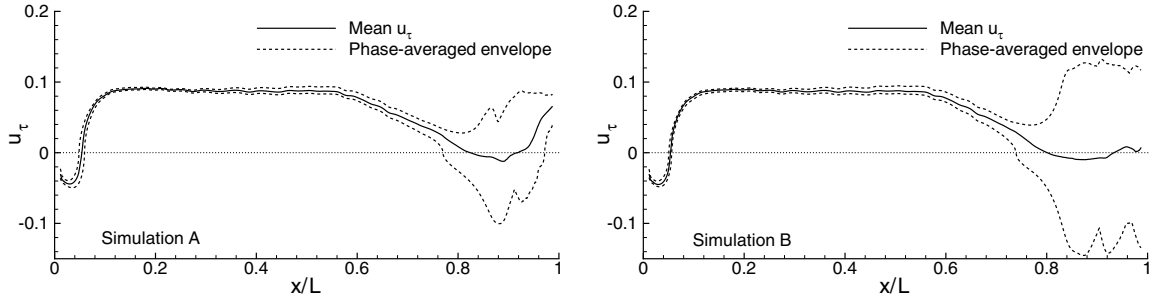

Fig. 10. Mean friction velocity and its phase-averaged envelope of Simulations A and B.

appear. The variation of the phase-averaged signal in Simulation B is significantly larger that the corresponding variation in Simulation A. The small-scale fluctuations carried by the wakes of Simulation A appear to be quite effective in reducing the variation in u_τ. An explanation for this is that the advanced transition to turbulence in Simulation A, which is triggered by these small-scale fluctuations, rapidly destroys the coherence of the KH-rolls, which are the most likely cause of the observed variation in the phase-averaged u_τ.

On the pressure side, because of the favourable streamwise pressure-gradient (with an acceleration parameter K larger than 3×10^{-5} downstream of $x/L=0.363$), the boundary-layer flow is found to remain laminar at all times. The snapshot in Fig. 11 shows the presence of longitudinal vortical structures along the pressure side of the turbine blade in Simulation A (see also Wu and Durbin, 2001; Wissink, 2003). These structures appear to be generated inside the passage and subsequently lay down on the surface. In particular, these vortices are not Goertler vortices. This is evidenced by the fact that corresponding vortical structures are not found to be present in Simulation B.

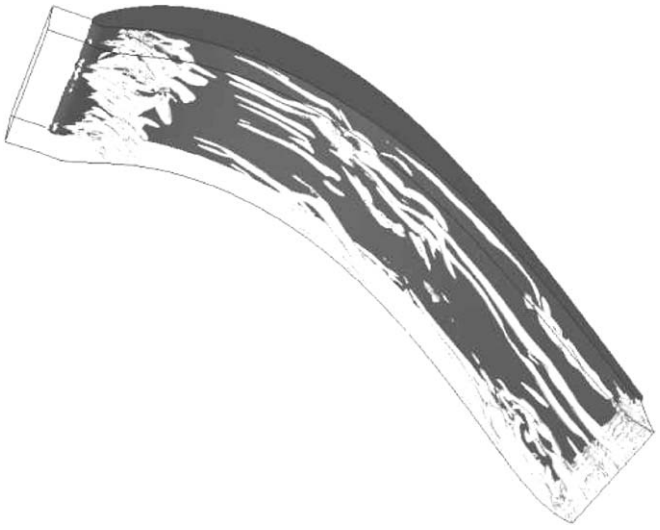

Fig. 11. Simulation A: Longitudinal vortical structures along the pressure side of the blade. The structures are visualised using the λ_2-criterion of Jeong and Hussain (1995).

Instead, the flow along the pressure side is found to remain virtually undisturbed, showing that for the formation of these longitudinal structures along the pressure side, it is necessary that the wake contains fluctuations.

3. Discussion and conclusion

Direct numerical simulations have been performed of incompressible flow in the T106A low-pressure turbine cascade with incoming wakes. In one of the simulations small-scale fluctuations were removed from the wake before it enters the inflow plane of the turbine cascade. Comparing the two simulations allows one to differentiate between the effects related to the large-scale motion of the wakes and the effects related to the presence of small-scale disturbances carried by the wakes. The relatively large inflow angle, combined with the relatively low Reynolds number causes the flow to separate along the downstream half of the suction side. A comparison of the two simulations leads to the following conclusions:

- As also observed in the experiments of Stieger and Hodson (2003), in both simulations a Kelvin–Helmholtz (KH) instability of the separated shear layer is found to be triggered by the impinging wakes. Hence, the presence of small-scale fluctuations does not affect this initial inviscid instability mechanism. Further transition to turbulence, which mainly happens inside the KH-rolls, is found to depend on the presence of small-scale disturbances: Without such disturbances the suction side boundary layer flow is found to remain two-dimensional—and hence laminar—almost up to the trailing edge. As a consequence, the onset of transition in Simulation A is located farther upstream than in Simulation B and only in Simulation A the wakes are able to intermittently suppress separation.
- The small-scale fluctuations in Simulation A are found to be very effective in destroying the KH-rolls, resulting in a drastic reduction in the variation of the friction velocity along the downstream half of the suction side as compared to Simulation B.
- Whether or not production of kinetic energy takes place at the apex of the deformed wake as it is convected through the passage between blades is found to depend

fully on the presence of small-scale disturbances. Without such disturbances there is no production of kinetic energy at this location.

- Compared to Simulation B, the phase-averaged flowfield in Simulation A shows virtually no large-scale structures to be present in the near wake of the blade. This can be explained by the constant supply of turbulent flow stemming from the suction side of the turbine blade which merges with the wake downstream of the trailing edge and subsequently hinders the formation of large-scale structures.
- The longitudinal vortical structures which were found to be formed along the pressure side by Wu and Durbin (2001) and Wissink (2003), are a direct effect of impinging small-scale fluctuations carried by the wakes. Once such fluctuations are removed from the wakes, the structures are found to disappear.

Acknowledgements

The authors would like to thank the German Research Foundation (DFG) for funding this project and the Steering Committee of the Super Computing Facilities in Bavaria (HLRB) for granting computing time on the Hitachi SR8000-F1 at the Leibniz Computing Centre (LRZ) in Munich.

References

Breuer, M., Rodi, W., 1996. Large eddy simulation for complex turbulent flows of practical interest. In: Hirschel, E.H. (Ed.), Flow simulation with High-Performance Computers II, Notes in Numerical Fluid Mechanics, vol. 52. Vieweg-Verlag, Braunschweig.

Jeong, J., Hussain, F., 1995. On the identification of a vortex. J. Fluid Mech. 285, 69–94.

Kalitzin, G., Wu, X., Durbin, P.A., 2002. DNS of fully turbulent flow in a LPT passage. In: Rodi, W., Fueyo, N. (Eds.), Engineering Turbulence Modelling and Experiments, vol. 5. Elsevier, pp. 741–750.

Liu, X., Rodi, W., 1994a. Velocity measurements in wake-induced unsteady flow in a linear turbine cascade. Exp. Fluids 17, 45–58.

Liu, X., Rodi, W., 1994b. Surface pressure and heat transfer measurements in a turbine cascade with unsteady oncoming wakes. Exp. Fluids 17, 171–178.

Michelassi, V., Wissink, J.G., Rodi, W., 2002. Analysis of DNS and LES of flow in a low-pressure turbine cascade with incoming wakes and comparison with experiments. Flow, Turbul. Combust. 69, 295–329.

Michelassi, V., Wissink, J.G., Fröhlich, J., Rodi, W., 2003. LES of flow around a low-pressure turbine blade with oncoming wakes. AIAA J. 41, 2143–2156.

Raverdy, B., Mary, I., Sagaut, P., Liamis, N., 2003. High-resolution large-eddy simulation of flow around low-pressure turbine blade. AIAA J. 41, 390–397.

Rhie, C.M., Chow, W.L., 1983. Numerical study of the turbulent flow past an airfoil with trailing edge separation. AIAA J. 21, 1525–1532.

Schulte, V., Hodson, H.P., 1998. Unsteady wake-induced boundary layer transition in high-lift LP turbines. ASME J. Turbomach. 120, 28–35.

Stadtmüller, P., 2002. Grenzschichtentwicklung und Verlustverhalten von hochbelasteten Turbinengittern unter dem Einfluss periodisch instationärer Zuströmung, Ph.D. Thesis. U. der Bundeswehr München, Germany.

Stieger, R., Hodson, H.P., 2003. The transition mechanism of highly loaded LP turbine blades. In: Proceedings ASME Turbo Expo 2003, paper no. GT2003-38304.

Stieger, R., Hodson, H.P., 2005. Convection of a turbulent bar wake through a low-pressure turbine cascade. ASME J. Turbomach. 127, 388–394.

Stieger, R., Hollis, D., Hodson, H.P., 2003. Unsteady surface pressures due to wake-induced transition in a laminar separation bubble on a LP turbine cascade. In: Proceedings ASME Turbo Expo 2003, paper no. GT2003-38303.

Wissink, J.G., 2003. DNS of separating, low Reynolds number flow in a turbine cascade with incoming wakes. Int. J. Heat Fluid Flow 24, 626–635.

Wu, X., Jacobs, R.G., Hunt, J.C.R., Durbin, P.A., 1999. Simulation of boundary layer transition induced by periodically passing wakes. J. Fluid Mech. 398, 109–153.

Wu, X., Durbin, P.A., 2001. Evidence of longitudinal vortices evolved from distorted wakes in a turbine passage. J. Fluid Mech. 446, 199–228.

Zhang, X.F., Hodson, H.P., 2004. The combined effects of surface trips and unsteady wakes on the boundary layer development of an ultra high-lift LP turbine blade. In: Proceedings ASME Turbo Expo 2004, paper no. GT2004-53081.